ISSN (Print) 1226-1750
ISSN (Online) 2233-6656
Journal of Magnetics 23(3), 386-391 (2018) https://doi.org/10.4283/JMAG.2018.23.3.386

Leakage Flux Reduction Applying Rib-less Structure in V-shape Interior Permanent Magnet Synchronous Motor

Myung-Hwan Yoon[1], Jae-Han Sim[2], Ji-Min Kim[3], Myung-Seop Lim[4], Jae-Woo Jung[5], and Jung-Pyo Hong[2]*

[1]Hyundai Motor Company, Hwaseong 18280, Korea
[2]Department of Automotive Engineering, Hanyang University, Seoul 04763, Korea
[3]Motor R&D Group, Digital Appliances, Samsung Electronics, Suwon 16677, Korea
[4]School of Mechanical Engineering, Yeungnam University, Gyeongbuk 38541, Korea
[5]Hyundai Mobis, Yong-in 16891, Korea

(Received 18 March 2018, Received in final form 4 September 2018, Accepted 4 September 2018)

Permanent magnet machines are suitable for Hybrid Electric Vehicle (HEV) and Electric Vehicle (EV) application because of its superior torque density, high efficiency and small size. Especially, Interior Permanent Magnet Synchronous Motor (IPMSM) is an appropriate type because an air-gap flux density can be maximized and reluctance torque is enhanced using the saliency of rotor shape. However, a leakage flux generated in a magnetic rib which circulates inside the rotor and causes the decrease of the air-gap flux density. In this paper, an improved rotor structure is proposed where the magnetic ribs are removed and centre bridges are added for the mechanical stiffness. The air-gap flux density increased because two leakage paths are reduced to one path which are the magnetic ribs and the centre bridge respectively. In addition, the mechanical strength are analysed and compared. Finally, the improved model is manufactured and test is conducted for the verification.

Keywords : interior permanent magnet synchronous motor, leakage flux, magnetic rib

1. Introduction

These days fuel economy of vehicle is significant, therefore many studies are conducted to realize the high fuel economy for the eco-friendly vehicle such as a hybrid car and an electric car. One of methods to improve the fuel economy is to increase energy efficiency of traction device and another one is a reduction in vehicle weight to reduce the loss. Dozens of electric motors are applied to the hybrid car and the electric car which are considerably heavy. Accordingly, minimizing the motor size is required for the reduction of motor weight and designing motor of high torque density. Recently, motors are applied for the operation of regenerative braking system in a hybrid vehicle. Conventional hydraulic brake booster is replaced by a motor, therefore the weight and the volume of the system can be reduced. Furthermore, the volume of system can be additionally reduced as the torque of motor increases. A method of increasing flux generated from the field is an effective way to improve a magnetic torque for the higher torque density of Surface-mounted Permanent Magnet Synchronous Motor (SPMSM), however there is a limit of magnet usage. On the other hand, in case of IPMSM, magnets can be arrayed as V-shape in the rotor which can increase the flux of field and reluctance torque can be also used to improve the torque density [1, 2]. However, leakage flux is generated in magnetic ribs of IPMSM which circulates inside the rotor and causes a decrease of the air-gap flux density. There are many studies for the reduction of the leakage flux and dealing with the reduction in the thickness or increase in the length of magnetic ribs [3, 4]. But these methods cannot be applied to a small-size motor because the thickness of magnetic ribs should be greater than a manufacturing limit size. This manufacturing limit can be supplemented by a new structure which is a rib-less structure. In this paper, the improved rotor structure for vehicle application is proposed where magnetic ribs are removed and this can be applied to the small-size motor. As the magnetic ribs on both sides of permanent magnets

*Corresponding author: Tel: +82-2-2220-4466
Fax: +82-2-2220-4465, e-mail: hongjp@hanyang.ac.kr

are removed, leakage flux can be significantly reduced. However, centre bridges are added to the rotor for the mechanical stiffness. As a result, a structural safety is necessary to be checked because only one bridge must support two magnets where two magnetic ribs support in conventional model. In electromagnetic point of view, the flux density in the air-gap increased by the structure and the size of motor can be reduced which results in higher torque density. The leakage flux of the suggested motor is obtained by Finite Element Analysis (FEA) and performance of motor is predicted. In addition, the mechanical strength is analyzed and compared to the conventional rotor structure. Finally, the improved motor is manufactured and the performance of motor is verified by test.

2. Design of motor

2.1. Specification of motor

Motor specification of the braking system is presented in Table 1. The required torque of the system is 3.7 Nm and the maximum power is 450 W. The limit of stator outer diameter is 76 mm and stack length is 20 mm. IPMSM type is determined for the higher torque density compared to SPMSM.

2.2. Deciding pole and slot combination

Various combinations of pole and slot can be applied to the motor design and this paper deals with a concentrated winding application [5-8]. Applying the concentrated winding can reduce the size of motors compared to the distributed winding because of smaller end-turn height. On the other hand, V-shape magnet array can also increase the torque density of IPMSM where the usage of magnet can be increased within the same rotor size compared to the conventional I type magnet [9-13]. However, vibration and noise are critical issue for IPMSM on account of a small air-gap length. The combination of pole and slot affects winding factor, torque ripple, cogging torque, and vibration. Table 2 presents the comparison of parameters mentioned above among five different combinations. The winding factor of fundamental harmonic is related to the torque, fifth and seventh harmonics cause the torque ripple, and the least common multiple affects the cogging torque and torque ripple. The magnetic radial force distributions of the combinations are analyzed using the Maxwell stress tensor, as following equation. The radial force distributions are compared in Fig. 1 and determine the vibration mode of the motor which affects the rotary stability [14, 15]. In (1), P_{mr} is the radial magnetic pressure, B_{mv} and $B_{m\mu}$ are the magnetic flux densities excited by the stator harmonic and the rotor harmonic, respectively, and μ_0 is the magnetic permeability of the free space. Furthermore, the deflection of the stator core is proportional to an inverse function of fourth power of force order. In addition, radial force distributions are compared in Fig. 1 and well balanced distribution causes smaller vibration. As electromagnetic and mechanical characteristics are considered, 14 pole and 18 slot is determined.

$$P_{mr} = \frac{B_{mv} \bullet B_{m\mu}}{2\mu_0} \tag{1}$$

Table 1. Motor specification for braking system.

Items	Unit	Vale
Stator outer diameter	mm	76
Stack length	mm	20
Maximum torque	Nm	3.7
Maximum power	W	450

2.3. Design of conventional type motor

A conventional structure of two magnetic ribs is shown in Fig. 2 which performs the objective torque of 3.7 Nm. V-shape magnet type is applied to maximize the flux generated from the rotor. However, the stack length of this motor is 22 mm which is not satisfactory to the objective length of 20 mm. The leakage flux generated in the magnetic ribs is the cause of this dissatisfaction. The flux distribution of the conventional type is presented in Fig. 3 and the leakage flux can be verified. The leakage flux can be reduced by thin ribs, but there is a limit of rib thickness. In general, the thickness of the thinnest part of steel is the thickness of steel sheet as the pressing is

Table 2. Combination of pole and slot.

Pole / Slot	1st winding factor	5th winding factor	7th winding factor	Least Common Multiple	Force order
6 / 9	0.866	0.866	0.866	18	3
8 / 9	0.945	0.140	0.061	72	4
10 / 12	0.933	0.067	0.067	60	2
12 /15	0.910	0	0.088	60	3
14 / 18	0.902	0.038	0.136	126	4

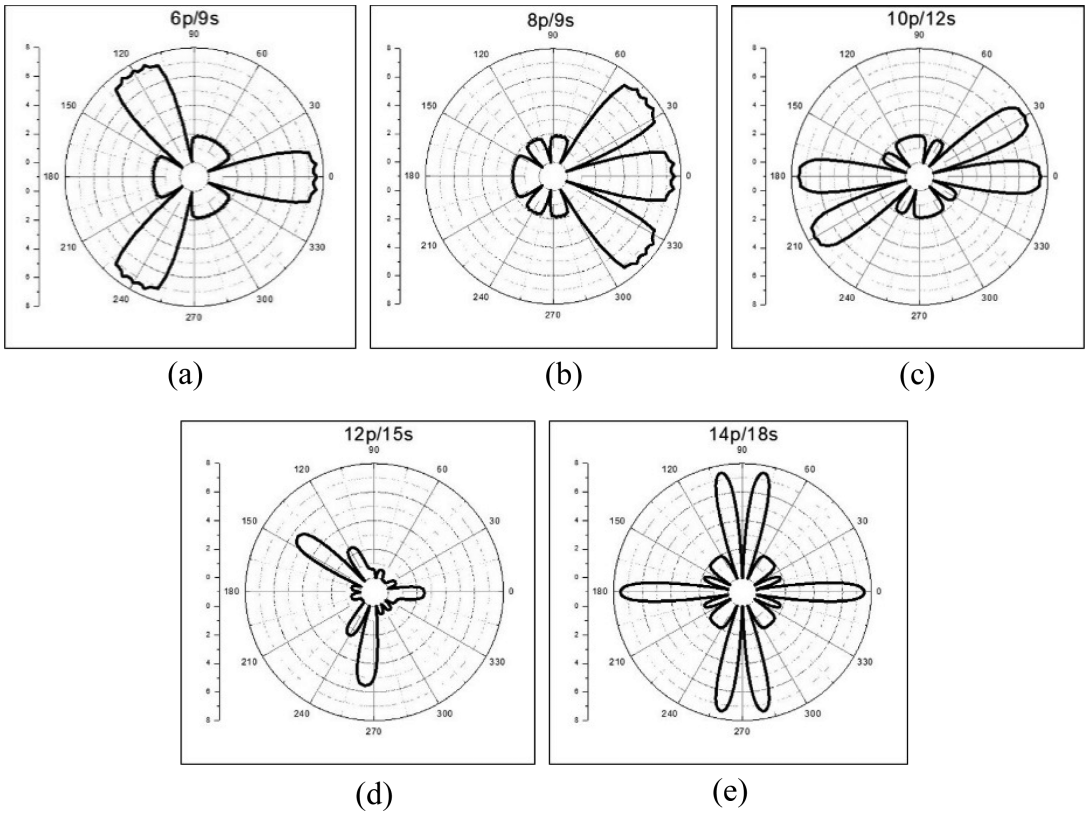

Fig. 1. Distribution of radial force. (a) 6 pole 9 slot (b) 8 pole 9 slot (c) 10 pole 12 slot (d) 12 pole 15 slot (e) 14 pole 18 slot

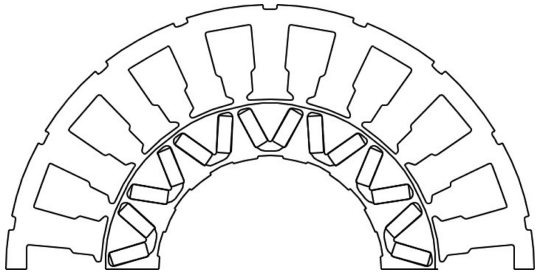

Fig. 2. Conventional type model.

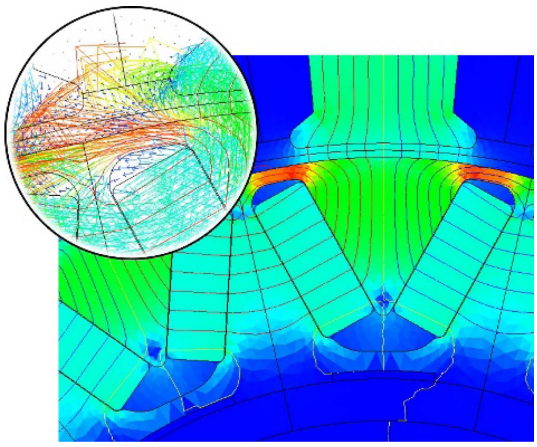

Fig. 3. (Color online) Flux distribution of conventional type model.

applied. The thickness of steel material is 0.5 mm and the limit of rib is also 0.5 mm. As thinner thickness of steel is applied, a manufacturing cost rises and the life span of press mold decreases. Therefore, a general V-shape type structure cannot satisfy the requirement of the braking system. In this paper, an improved structure for the reduction of leakage flux in magnetic ribs is suggested to solve the problem.

3. Rib-less Structure

3.1. Rib-less structure

The improved structure which is the rib-less rotor is

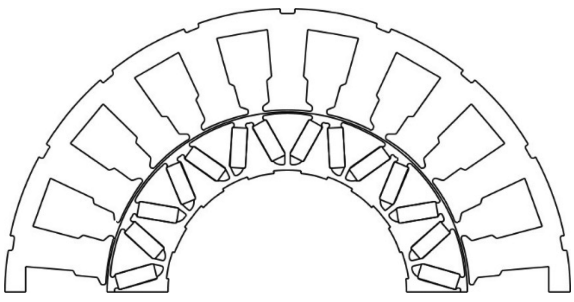

Fig. 4. Rib-less type model.

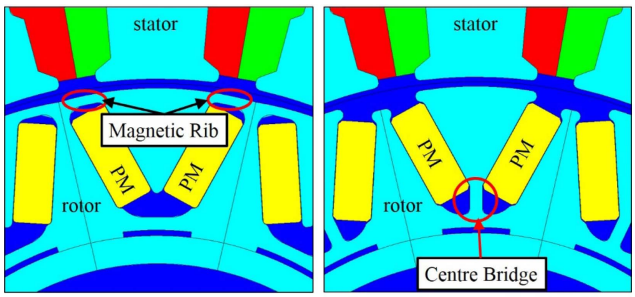

Fig. 5. (Color online) Structural comparison (a) Conventional structure (b) Rib-less structure.

presented in Fig. 4. The magnetic ribs on both side of permanent magnets in the conventional model are removed as shown in Fig. 5. The role of magnetic ribs for the mechanical stiffness is substituted with a centre bridge between two magnets. Much of leakage flux is generated at magnetic ribs in the conventional structure, but the leakage flux is concentrated in the centre bridges in the rib-less structure. Therefore, the leakage flux is reduced relatively. The flux distribution of the rib-less model is illustrated in Fig. 6 and the concentration of the leakage flux in the bridges can be checked.

3.2. Comparison between conventional model and rib-less model

The linkage flux of the rib-less model on no-load condition increases by 9 % compared to that of the conventional model with the same stack length as shown in Fig. 6. Furthermore, torque performances of two models are compared in Fig. 7 where saliency ratios of both motors are the same which is 1.3. An armature current of 50A_{rms} which is the current limit and a current

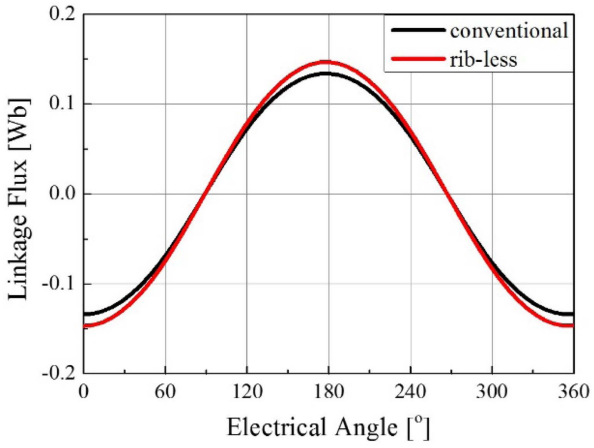

Fig. 6. (Color online) Linkage flux on no-load condition.

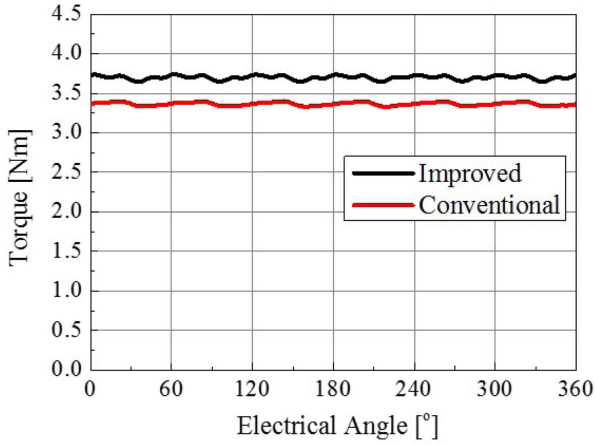

Fig. 7. (Color online) Torque comparison between conventional and improved model.

phase angle of 12° are the analysis conditions. As a result, torques of the improved model and the conventional model are 3.7 Nm and 3.4 Nm respectively. However, torque ripples of the models are 2.5 % and 2.1 % respectively which is the similar level. The torque increased approximately 9 % because of the linkage flux increase. Consequently, the improved model satisfies the requirement of the braking system within the size limit. In addition, the thickness of centre bridge in the improved model is 0.7 mm which can be easily manufactured and pressed.

3.3. Structural analysis

As mentioned above, the centre bridges supports the magnets in the rib-less model [16]. Therefore, the structural stiffness is required to be verified for the safety. Two ribs of 0.5 mm are supporting the structure in the conventional model but the two ribs are substituted with one centre bridge of 0.7 mm in the rib-less model, therefore the verification of bridge stiffness is required. Safety is confirmed by structural analysis with two models. The maximum speed of motor for the requirement is 3000 rpm, however the condition of structural analysis is 4000 rpm. Because the nominal voltage of battery used in the motor design is 12 V but the maximum voltage is approximately 14 V which means that the motor can be operated under 14 V in certain cases. Boundary conditions for each model are shown in Fig. 8. Assuming the worst circumstance, boundary conditions between magnet and structures are frictionless. In order to insert the magnet into rotor core, it should have a dimensional tolerance between the magnet and the rotor core. In general, the space caused by the tolerance is filled with an industrial adhesive to increase the strength and solidity

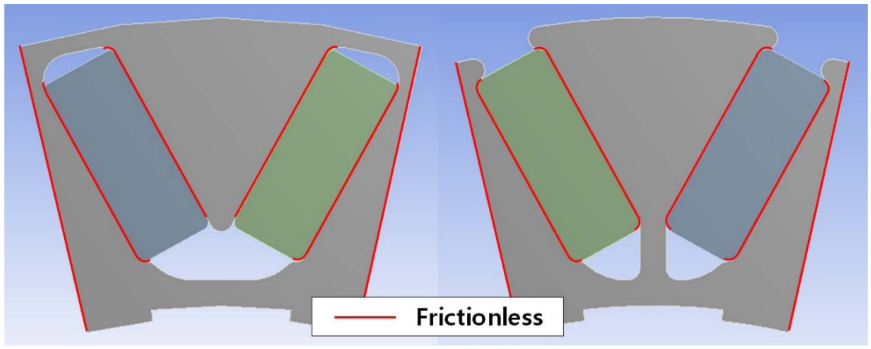

Fig. 8. (Color online) Boundary condition.

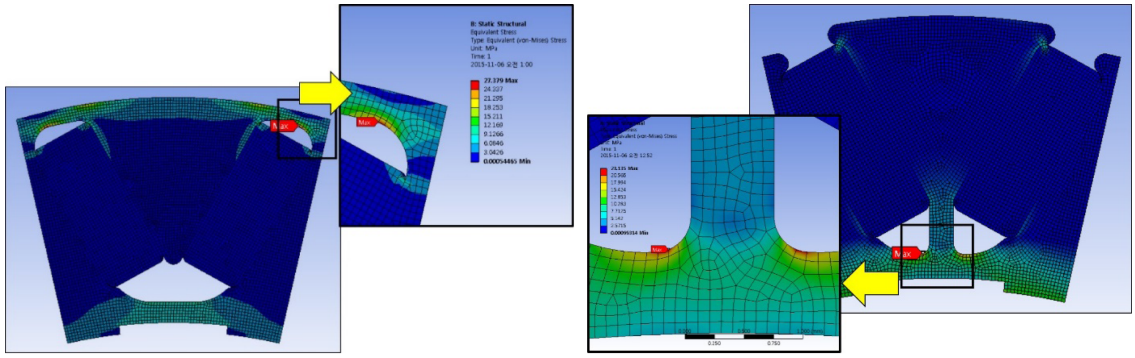

(a) (b)

Fig. 9. (Color online) Stress distribution (a) Conventional model (b) Rib-less model.

between the PM and the core. However, the bonding strength becomes weaker as time passes and this strength is not permanently constant [17]. Hence, the frictionless condition for the boundary condition is reasonable. The analysis results for the models are presented in Fig. 9. The maximum stress of the conventional model is 27.4 MPa and the improved model is 23.1 MPa. Yield stress of material in two models is 410 MPa and the safety factor can be calculated by following equation [18]. Safety factor of the conventional model is 15.0 and the improved model is 17.7, which means that the safety factor of rib-less model is improved by 18 % compared to the conventional model.

$$\text{Factor of safety} = \frac{\text{Yield strength}}{\text{Maximum stress}} \tag{2}$$

4. Test Results

The manufactured rotor core of the improved model is

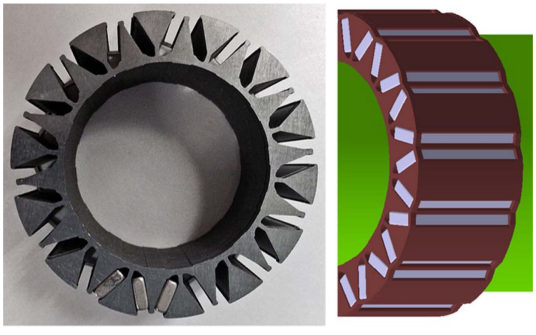

(a) (b)

Fig. 10. (Color online) Rotor core of rib-less model. (a) Manufactured rotor core (b) 3-dimensional model.

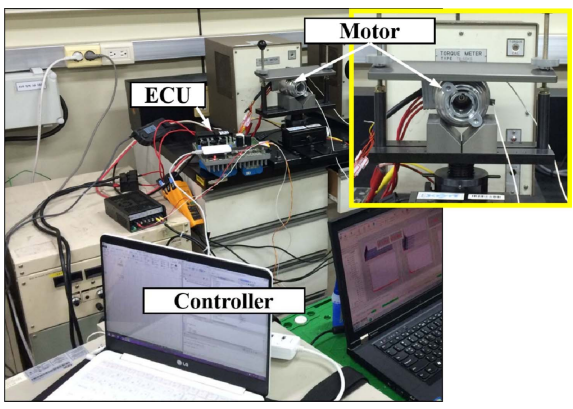

Fig. 11. (Color online) Configuration of test.

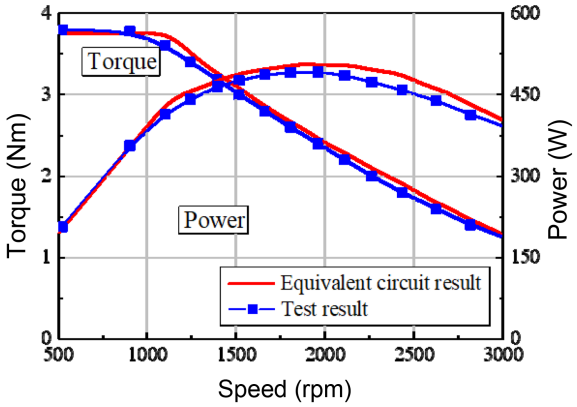

Fig. 12. (Color online) Torque-speed-power curves of rib-less model.

presented in Fig. 10(a). Safety of the braking system is significantly important because it has a great influence on driver's life. The safety is secured by the structural analysis previously, however two different shape of steel sheets are attached to the both ends of stack for the possible defect. The two steel sheets are connected to the upper part of magnet which is similar to the conventional model as shown in Fig. 10(b). These steel sheets play the role of prevention of the scattering phenomenon by the crack of magnet. The leakage flux generated from the two additional steel sheet is small enough to be neglected. Finally, a performance test of the manufactured rib-less model is conducted. Configuration of performance measurement equipment is presented in Fig. 11. Torque-speed-power curves of the rib-less model are measured, and the results of equivalent circuit and test are shown in Fig. 12.

5. Conclusion

In this paper, a high torque density motor is designed which satisfies the requirement of the braking system. Improved model is designed by V-type IPMSM for the high torque density. Combinations of pole and slot number are compared to decide the appropriate one for the higher torque, small torque ripple and vibration which is the demerit of IPMSM. The leakage flux generated in the magnetic ribs is the cause of lower performance in the conventional structure and this is improved in the suggested rotor structure. This rotor is composed of the centre bridges between magnets substituting the magnetic ribs on the both side of magnets in the conventional rotor. A structural analysis is conducted for the safety and performance test is also conducted for the verification. In the paper, a new structure for V-shape type IPMSM is suggested where magnetic ribs are removed and centre bridges are added. This structure is expected to be applied to the small-size rotor whose magnetic ribs are relatively thin. As the rib-less structure is used, 10 or more percentage of torque is obtained which results in higher torque density or smaller size.

References

[1] L. Fang, J. W. Jung, J. P. Hong, and J. H. Lee, IEEE Trans. Magn. **44**, 4393 (2008).
[2] D. G. Dorrell, A. M. Knight, and M. Popescu, IEEE Trans. Magn. **47**, 3016 (2011).
[3] M. Cirani, S. Eriksson, and J. Thunberg, IEEE Trans. Ind. Appl. **50**, 1847 (2014).
[4] R. Akaki, Y. Takahashi, K. Fujiwara, M. Matsushita, N. Takahashi, and M. Morita, IEEE Trans. Magn. **49**, 2335 (2013).
[5] H. J. Kim, D. J. Kim, and J. P. Hong, IEEE Trans. Magn. **50**, 7019504 (2014).
[6] Z. Q. Zhu, D. Wu, and X. Ge, IEEE Trans. Energy Convers. **31**, 1192 (2016).
[7] G. Verez, G. Barakat, and Y. Amara, IEEE Trans. Magn. **51**, 8101104 (2015).
[8] T. Sun, J. M. Kim, G. H. Lee, J. P. Hong, and M. R. Choi, IEEE Trans. Magn. **47**, 1038 (2011).
[9] W. Ren, Q. Xu, and Q. Li, IEEE Trans. Magn. **51**, 8113704 (2015).
[10] W. Ren, Q. Xu, Q. Li, and L. Zhou, IEEE Trans. Magn. **52**, 8104105 (2016).
[11] X. Zhu, Z. Shu, L. Quan, Z. Xiang, and X. Pan, IEEE Trans. Magn. **52**, 8205508 (2016).
[12] P. W. Huang and M. C. Tsai, IEEE Trans. Magn. **49**, 2311 (2013).
[13] Y. J. Zhou and Z. Q. Zhu, IEEE Trans. Magn. **49**, 3834 (2013).
[14] J. Boisson, F. Louf, J. Ojeda, X. Mininger, and M. Gabsi, IEEE Trans. Ind. Electron. **61**, 3081 (2014).
[15] H. Y. Yang, Y. C. Lim, and H. C. Kim, IEEE Trans. Ind. Electron. **60**, 4292 (2013).
[16] E. C. Lovelace, T. M. Jahns, T. A. Keim, and J. H. Lang, IEEE Trans. Ind. Electron. **60**, 4292 (2013).
[17] J. W. Jung, B. H. Lee, D. J. Kim, J. P. Hong, J. Y. Kim, S. M. Jeon, and D. H. Song, IEEE Trans. Magn. **48**, 911 (2012).
[18] J. M. Kim, S. H. Chai, M. H. Yoon, and J. P. Hong, IEEE Trans. Magn. **51**, 205204 (2015).